Numerical Simulation of the Gulf Stream and the Deep Circulation

HYUN-CHUL LEE* and GEORGE L. MELLOR

AOS Program, Princeton University, Princeton, NJ 08544-0710, U.S.A.

The Gulf Stream system has been numerically simulated with relatively high resolution and realistic forcing. The surface fluxes of the simulation were obtained from archives of calculations from the Eta-29 km model which is an National Center for Environment Prediction (NCEP) operational atmospheric prediction model; synoptic fields are available every 3 hour. A comparison between experiments with and without surface fluxes shows that the effect of the surface wind stress and heat fluxes on the Gulf Stream path and separation is closely related to the intensification of deep circulations in the northern region. Additionally, the separation of the Gulf Stream and the downslope movement of the Deep Western Boundary Current (DWBC) are reproduced in the model results. The model DWBC crosses under the Gulf Stream southeast of Cape Hatteras and then feeds the deep cyclonic recirculation east of the Bahamas. The model successfully reproduces the cross-sectional vertical structures of the Gulf Stream, such as the asymmetry of the velocity profile, and this structure is sustained along the downstream axis. The distribution of Root Mean Square (RMS) elevation anomaly of the model shows that the eddy activity of the Gulf Stream is realistically reproduced by the model physics. The entrainment of the upper layer slope current into the Gulf Stream occurs near cross-over; the converging cross-stream flow is nearly barotropic.

1. Introduction

With the increase of computational resources, it is possible to prognostically reproduce ocean circulations with higher horizontal and vertical resolution. This is particularly important for models of the Gulf Stream, which plays an important role in interior ocean dynamics but also in the coastal regions. Because of its huge heat and salt transport, the accurate modelling of Gulf Stream behavior is important to the simulation of the entire Atlantic Ocean (Dengg *et al.*, 1996).

Beckmann *et al.* (1994) investigated the effects of increased horizontal resolution in a simulation of the North Atlantic Ocean, from $1/3° \times 2/5°$ to $1/6° \times 1/5°$, in which the northward bump of the Gulf Stream occurs near the Cape Hatteras. Ezer and Mellor (1994) performed out prognostic numerical studies for the North Atlantic Ocean using a sigma coordinate ocean model (Blumberg and Mellor, 1987) with varying horizontal resolution of 20–100 km. Even though successful model results were ob-

tained for major ocean features of the North Atlantic, the prognostic models exhibited the northward shifting of the Gulf Stream at Cape Hatteras.

A somewhat simplistic diagram is presented in Fig. 1 (Mellor, 1996). In this paper we define the Northern Slope Current (NSC) as being comprised of the Upper Slope Current (USC; approximately 0–1000 m depth) and the underlying Deep Western Boundary Current (DWBC; deeper than 1000 m). The USC turns south-eastward north of Cape Hatteras and is entrained into the Gulf Stream. The DWBC flows under the Gulf Stream and proceeds southward with possible entrainment and detrainment. We define the Northern Cyclonic Gyre (NCG) as that formed by the NSC in the north and the Gulf Stream in the South; one is tempted instead to use the label Northern Recirculation Gyre, but this would not coincide with the same label defined by Hogg (1986).

Previous observational studies (Hogg, 1986; Pickart and Smethie, 1993; Pickart, 1994) have revealed an interaction between the Gulf Stream and deep circulations such as the Deep Western Boundary Current (DWBC). The Hogg and Stommel's (1985) analytical model of the relation between the Gulf Stream and the DWBC showed

---
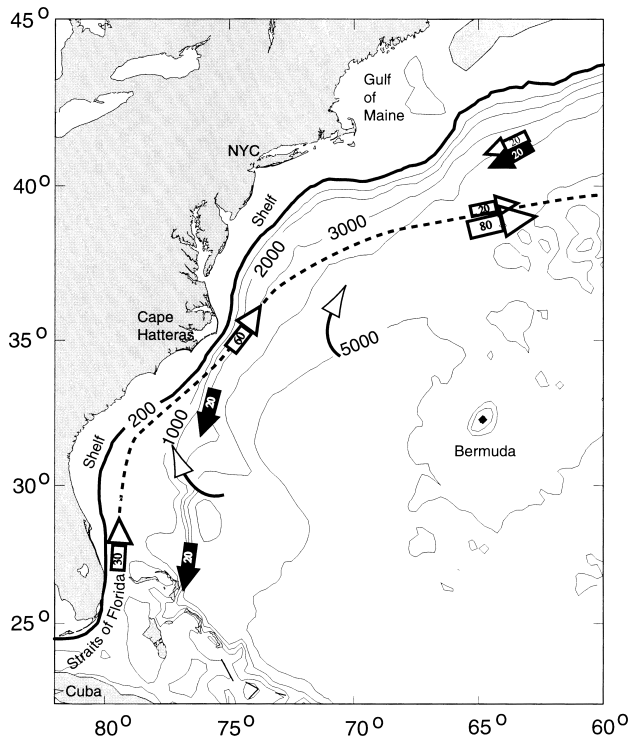
* Corresponding author. E-mail: lhc@splash.princeton.edu

Fig. 1. Near surface flow (0–1000 m, open arrows) and deep water flow (deeper than 1000 m, solid arrows). The contour interval of water depth is 1000 m; the exception is the heavy contour denoting the 200 m isobath and marking the outer edge of the continental shelf. Climatological path of the Gulf Stream axis is denoted by the heavy dashed line. (Adapted from Mellor, 1996.)

that the offshore portion of the Gulf Stream is compatible with downslope movement of the DWBC under the constraint of uniform potential vorticity. Pickart and Smethie (1993) investigated the kinematics in which the DWBC crosses the Gulf Stream at Cape Hatteras and suggested that the upper layer of the DWBC decreases the potential vorticity of the Gulf Stream by entrainment, which induces a more southerly point of separation.

The numerical experiments by Thompson and Schmitz (1989), using a two layer model, indicated that the mean axis of the Gulf Stream moves to the south, and the northward overshooting of the Gulf Stream separation is reduced when the input boundary transport of their model DWBC at 45°N was increased. Ezer and Mellor (1992) showed that the NCG north of the Gulf Stream is necessary to Gulf Stream separation at Cape Hatteras. Spall (1996a, b) looked at the dynamics of the Gulf Stream and DWBC crossover using a regional ocean layer model. He found that the entrainment and mixing of the upper slope water have a significant impact on the separation point and mean path of the Gulf Stream. He also showed

a decadal oscillation in the Gulf Stream/DWBC system, which is caused by the interaction between the low potential vorticity DWBC water and the eddy flux that maintains the interior recirculation gyre.

In this paper a numerical simulation of the Gulf Stream System, including the Gulf of Mexico, is executed using a regional Princeton Ocean Model. The NCEP model does not include the Gulf of Mexico and has about a 50% larger grid spacing. The purpose of this paper is to simulate major features of the Gulf Stream System prior to the imposition of SST and altimetric data assimilation. We investigate the relation between the Gulf Stream and the lower layer circulation, especially the variability of the DWBC and its effect on the Gulf Stream separation, and the simulated vertical structure of the Gulf Stream.

Two models have been executed, one without sea surface fluxes and the other an experiment with 3-hourly atmospheric fluxes. We immediately demonstrate that surface forcing is necessary for a realistic Gulf Stream morphology and most of the paper is thereafter devoted to the case with surface forcing.

2. Model Configuration

The Princeton Ocean Model (POM) used in this study is a free surface, primitive equation ocean model (Blumberg and Mellor, 1987). The vertical structure of this model is represented by a bottom-following, sigma coordinate system which can simulate bottom boundary layers as well as the surface Ekman layers. The horizontal grid is defined on curvilinear orthogonal coordinates. The vertical diffusivity is calculated from a turbulence closure model (Mellor, 1973; Mellor and Yamada, 1982). Following Smagorinsky's formulation (Smagorinsky *et al.*, 1965), the horizontal viscosity of the model is proportional to the square of the grid size and horizontal velocity shear with a coefficient of 0.05. The horizontal diffusivity is one fifth of the viscosity. By the mode-splitting technique, free surface dynamics are included explicitly in this model. The governing equations and model physics are described by Mellor (1998).

Figure 2 shows the model grid (every fifth grid line is shown) and bottom topography. The topographic data is obtained from the updated ETOPO5 files. The model grid is defined so that the resolution of the model is high along the US eastern coast and the finest meshes are located near Cape Hatteras (about 8 km × 10 km). The vertical resolution of the model is 25 sigma levels; the negatives of 0.0, 0.0014, 0.0028, 0.0054, 0.0106, 0.0210, 0.0418, 0.0835, 0.1668, 0.2501, 0.3334, 0.4167, 0.5000, 0.5833, 0.6666, 0.7499, 0.8332, 0.9165, 0.9582, 0.9790, 0.9894, 0.9946, 0.9972, 0.9986, 1.0. This distribution of sigma levels is designed to resolve the dynamics of the bottom boundary layers as well as the surface boundary layers.
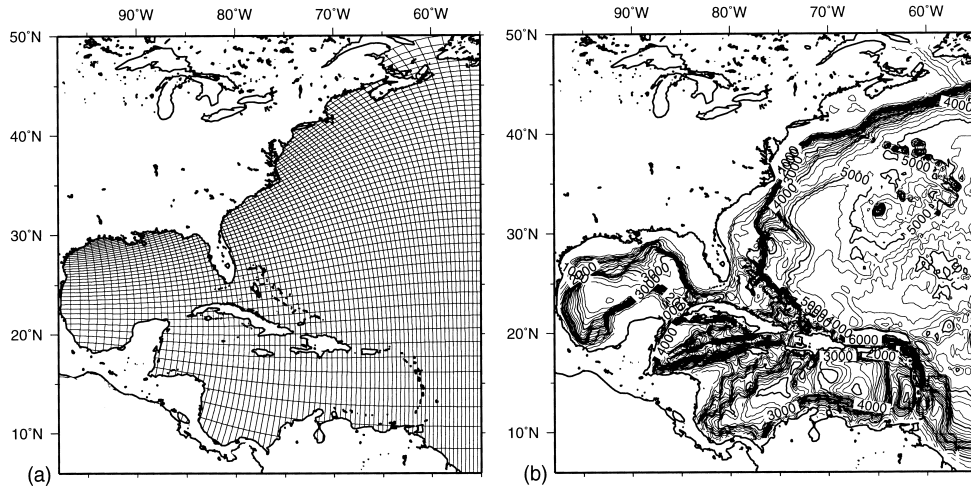
Fig. 2. (a) Orthogonal curvilinear coordinate grid with δx less than 8 km and δy less than 10 km around Cape Hatteras. For ease of visualization every fifth contour is plotted. (b) Bathymetry of the model basin with contour interval of 200 m.

The model basin has one open boundary along 55°W which cuts through the NCG of the Gulf Stream and the subtropical gyre of the north Atlantic Ocean. The transport along the open boundary is based on the averaged results of long-term current measurements near 55°W by Richardson (1985). Figure 3 shows the distribution of the transport stream function and barotropic (vertically averaged) velocity along the boundary. The transport of the Gulf Stream is 92 Sv (1 Sv = 10^6 m^{3}s^{-1}) near 39°N where the maximum barotropic velocity is 10 cm s^{-1}. The transport of the westward northern countercurrent is 37 Sv, and because of the shallow bottom topography, its maximum speed is over 20 cm s^{-1} near 46°N. Another 55 Sv flows eastward as the southern countercurrent south of the Gulf Stream. This fixed transport may limit the Gulf Stream transport variability of this simulation.

To investigate the effect of surface forcing, two cases of surface boundary conditions are applied here. In the first case the model is driven by steady lateral boundary forcing with no sea surface forcing. The second case is the full simulation wherein lateral boundary conditions for temperature and salinity are defined by monthly averaged fields from the GDEM data set (Teague *et al.*, 1990), and the surface fluxes of heat and momentum are calculated from the regional atmospheric Eta model of National Center for Environment Prediction (NCEP). There are several version of Eta models in terms of resolution, and we used the Eta-29 km model data. The method of coupling with the Eta model is the same as that described by Aikman *et al.* (1996). Atmospheric input data from the Eta model are short-wave solar radiation, downward long-wave radiation, potential air temperature, wind velocity, air humidity, surface pressure and precipitation rate, which are available every three hours. The wind
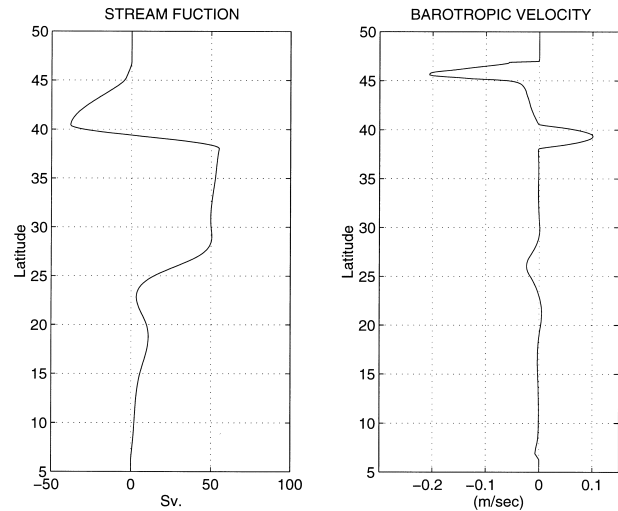

Fig. 3. Lateral boundary conditions of the transport stream function (left) and the barotropic velocity (right) along 55°W. This distribution of the transport stream function is based on observations by Richardson (1985) and the diagnostic calculation of Mellor *et al.* (1982). The peak of westward barotropic velocity at 46°N is coincident with shallow bottom topography.

stress and heat flux through the sea surface are calculated from these data together with the sea surface temperature and velocity of the ocean model by using stability-dependent bulk formulas. The Eta-29 km model region does not cover the southwestern region of the Caribbean Sea (Gulf of Mosquito) and the southeastern corner of the ocean model region. The atmospheric data over these regions were extrapolated by Laplacian iteration
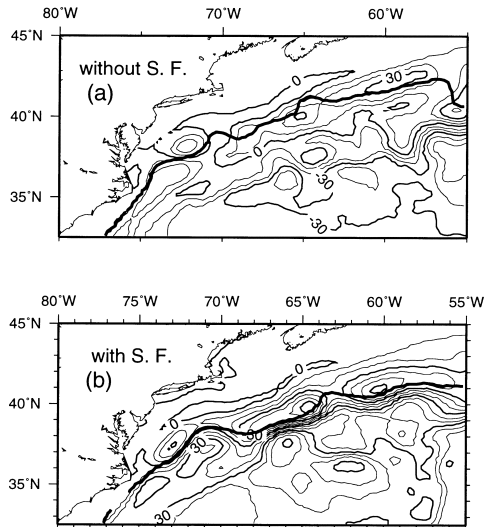
Fig. 4. (a) Annually averaged transport stream function fields of the 6th year from the experiment which has no surface fluxes and driven only by stationary lateral boundary condition. (b) Same but driven with surface fluxes from the three-hour interval Eta-29 km results and monthly temperature and salinity data at the lateral boundary. The C.I. of the stream function is 10 Sv. Thick solid lines are the annually averaged Gulf Stream path obtained from the model 12°C isotherm at 400 m depth.

Fig. 5. (a) Averaged net heat flux (from ocean to air) for six years. C.I. is 50 W/m^2. (b) Averaged wind stress curl for six years. (Solid line is positive and dashed line is negative.) C.I. is 20×10^{-7} N/m^{-3}.

from the border of the Eta-29 km region. The Eta-29 km data used here is available from October 1 1995 to May 31 1998. After that, model calculations are continued by repeating the surface data from June 1 1996 to May 31 1998.

The model starts from the temperature and salinity fields of the GDEM data set for October. To provide a near geostrophically adjusted velocity field, a diagnostic calculation, holding the initial density field constant, executes during the first five days.

3. Results

3.1 Ocean response for sea surface forcing

In Fig. 4, we compare the six year, annually averaged Gulf Stream path and stream function fields of the without-surface-forcing run and the with-surface-forcing run. The without-surface-forcing run is driven by the lateral transport and monthly climatologies of T and S along the open boundary. The with-surface-forcing run is driven by 3 hour surface heat flux and wind stress obtained from the Eta-29 km atmospheric prediction model and by monthly climatological T and S transection at the lateral open boundary, which are identical with that of the unforced experiment.
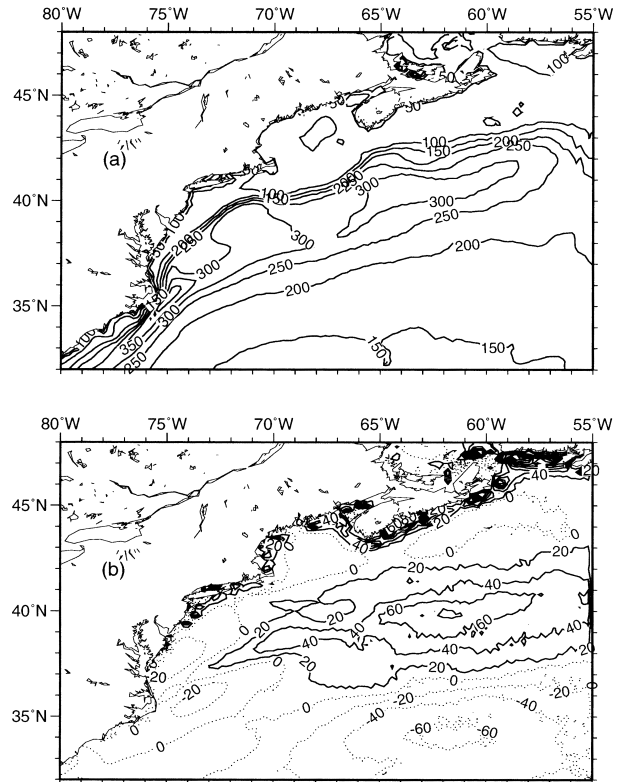
It is immediately obvious that surface forcing is nec-

essary for a realistic simulation; thus, the possibility that the interior flow might be dominated by the open boundary conditions is excluded. The 92 Sv transport boundary condition is essentially ignored in the model without surface forcing (Fig. 4(a)). In the extension region, the Gulf Stream path shifts to the north and is located near the edge of the continental shelf. This unrealistic distribution of the unforced Gulf Stream path affects the coastal circulation; warm and saline water occupies the northern area near the coastal region, and the northeastward coastal circulation strengthens. On the other hand, the Gulf Stream path (Fig. 4(b)) from the experiment with surface forcing conforms well with the observed path (Hansen, 1970; Shay *et al.*, 1995) and diagnostic transport calculations based on observed climatological density fields (Mellor *et al.*, 1982).

Figure 5 shows the annual average of the sea surface heat flux and the wind stress curl for the with-surface-forcing run. The large heat flux from ocean to air takes place in the Gulf Stream and the NCG region (north of the Gulf Stream), where the intense cooling (over 300 W m^2) occurs by the cold air and the warm ocean in winter. This cooling in the NCG region homogenizes and
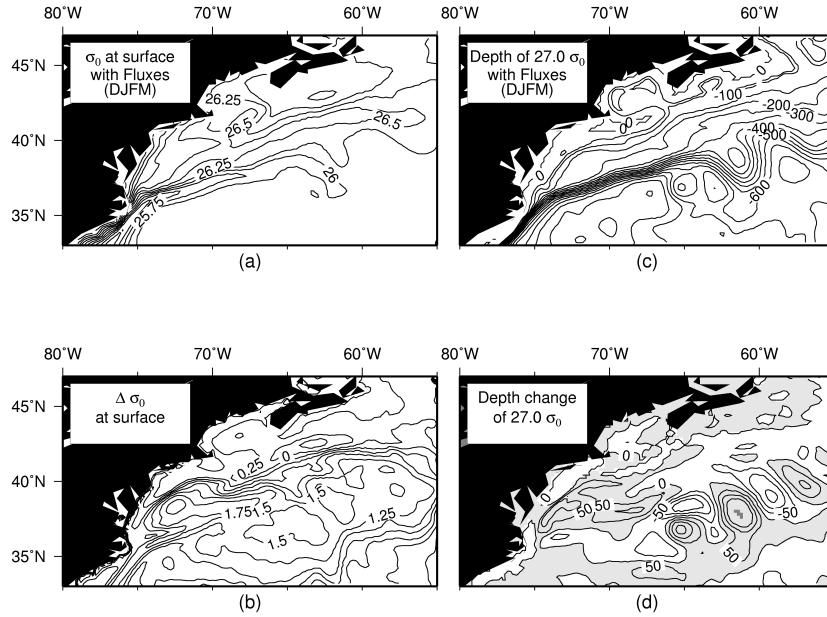
Fig. 6. (a) Averaged surface σ_0 distribution from the model with surface fluxes during the winter (from December 1996 to March 1997), and C.I. is 0.25 kg m^{-3}. (b) Difference of the surface σ_0 obtained by the subtraction of the model results without surface fluxes from the model result with surface fluxes. C.I. is 0.25 kg m^{-3}. (c) Depth of the isopycnal surface of $\sigma_0 = 27.0$. C.I. is 50 m. (d) Difference of the isopycnal surface depth of $\sigma_0 = 27.0$ between the model with surface fluxes and the model without surface fluxes. Hatching in the figure represent the region at which the isopycnal surface of $27.0\sigma_0$ from the model with fluxes is shallower than the model without fluxes. C.I. is 50 m.

deepens the upper layer ocean (Fig. 6(d)) and also increases the horizontal density gradient in the upper layer between the Gulf Stream and the slope water (Fig. 6(b)). For the thermal wind balance, the vertical velocity shear increases due to the increasing the horizontal density gradient, and in the upper layer the cyclonic transport of the NCG (including the upper layer transport of the Gulf Stream) is increased along the intensified density front.

It is clear that the mean wind stress curl of the with-surface-forcing run over the NCG region is positive (Fig. 5). This means that the regional wind forcing (positive wind stress curl) strengthens the cyclonic circulation over the NCG region. The intensification of the southward western rim of the NCG and the DWBC along the continental slope moves the separation position of the Gulf Stream further south (Thompson and Schmitz, 1989; Ezer and Mellor, 1992).

The intensified density front (actually cooler and denser northern slope water) blocks up the northward Gulf Stream along the continental slope and guides the Gulf Stream to separate from the coast. After the separation from the coast, vortex stretching occurs on arriving in the deeper region, and the vortex stretching enhances the separation of the current from the coast (Marshall and Tansley, 2001).

The southwestward transport maxima of the NCG from the experiment with surface forcing are about 60 Sv at 65°W and 61°W, and 35 Sv at 75°W at Cape Hatteras. The DWBC and the northern cyclonic gyre of the experiment without surface forcing are weaker than those of the with-surface-forcing one; the total transport of the NCG is about 20 Sv near 68°W and this is less than the half of the result from the with-surface-forcing run. The intensified NCG keeps the Gulf Stream path further south, as shown in the numerical study by Thompson and Schmitz (1989). This result is, of course, a consequence of the classical role of wind stress curl and, from an examination of mass fields, the wind stress and heat fluxes help to maintain the strong temperature and density contrasts between the Gulf Stream and the NCG and the concomitant baroclinic component of the flow.

Figure 6(a) shows the distribution of the averaged model surface σ_0 with surface forcing of the winter of 1996 (from December 1996 to March 1997). It is here that the outcrop of $26.25\sigma_0$ occurs in the northern region of the Gulf Stream and particularly the Mid Atlantic Bight. The surface water of the with-surface-forcing run in the Mid Atlantic Bight is denser by about 2 kg m^{-3} than the model without surface forcing (Fig. 6(b)). The averaged wind stress curl is positive (Fig. 5), and the Ekman pumping (upwelling) occurs in this region. Thus the refreshment takes place in the ventilated layer.
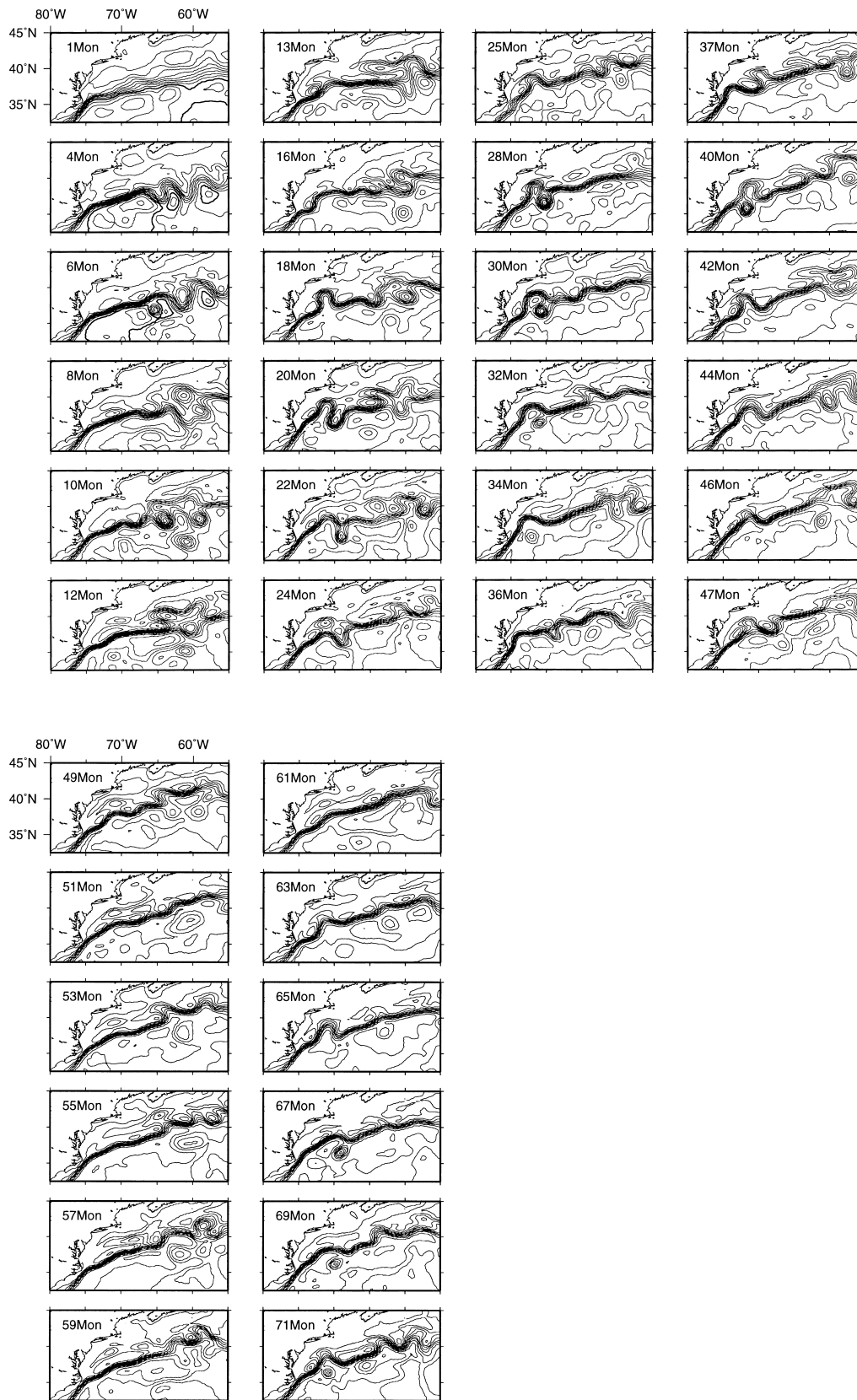
Fig. 7. Monthly averaged sea surface elevation fields for 6 years. Contour interval is 0.1 m.
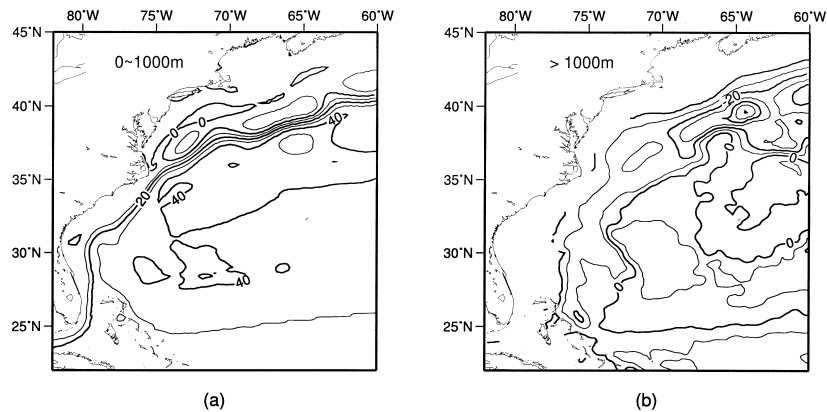
Fig. 8. Approximated transport stream function distributions from the two year averaged (year 5 and 6) velocity fields (a) in the layer of 0–1000 m, and (b) in the layer of 1000 m–bottom. Thick arrows represent the deep water flows which are labeled in Sverdrup unit. The C.I. of the stream function is 10 Sv.

Another considerable effect of the surface fluxes is shown in the change of the isopycnal surface (Fig. 5(d)); the $27.0\sigma_0$ surface of the model with surface fluxes is shallower by 100 m in the Mid Atlantic Bight.

Henceforth, we only examine the results from the experiment with surface heat fluxes and wind stress.

3.2 Evolution of the Gulf Stream

The morphology of the separation downstream of Cape Hatteras is an important index of the quality of the simulation of the Gulf Stream. In this section we look at Gulf Stream behavior in the region 55°W to 80°W and 33°N to 45°N, driven by the operational atmospheric Eta-29 km fields, and monthly climatological lateral boundary conditions for temperature and salinity.

Figure 7 shows the time evolution of the Gulf Stream path off Cape Hatteras represented by the monthly averaged surface elevation fields for 6 years. Because of the initial condition of the climatological temperature and salinity fields of the GDEM data set (Teague *et al.*, 1990) and 5-day diagnostic spin-up calculation, the Gulf Stream develops in the first month and subsequently exhibits the variability characteristic of this region.

For the first year, the Gulf Stream path off Cape Hatteras is straight and eddy activity occurs east of 65°W, near the New England Seamount chain; the path agrees with the climatologically averaged position of the observed Gulf Stream (Richardson, 1981; Hogg, 1983; Watts *et al.*, 1995). After the first year, meanderings of the Gulf Stream path occur west of 70°W and eddies and rings separate from and interact with the main stream. A cyclonic (cold) eddy forms from the steep trough at 72°W in month 27. This cold ring moves to the west with a speed of 2.4 cm s^{-1} which corresponds to the first mode Rossby wave and then merges into the Gulf Stream. The mean-

der ridge near 73°W is shifted to the west by the approaching cyclonic ring, and at the same time this eddy quickly dissipates. As a result, a bump of the Gulf Stream path occurs northward of the mean path in month 34. This anticyclonic bump is a typical overshooting pattern of Gulf Stream simulations (Beckmann *et al.*, 1994; Dengg *et al.*, 1996). The bump or ridge begins to fade in the 47th and 48th months. After month 47 in Fig. 7, the Gulf Stream straightens west of 65°W, and the Gulf Stream path recovers from the overshooting pattern to the observed path and this persists through years five and six.

3.3 Upper and lower circulations

Figure 8 shows the approximate transport stream function of the averaged circulation for two years (year 5 and 6) in the upper layer (0 to 1000 m) and lower layer (1000 m to the bottom). To a fair degree of approximation, we find that is possible to neglect vertical flow between layers and therefore a stream function for each layer may be defined in the model results. After separation from the coast, the transport of the Gulf Stream increases to 80 Sv, due to entrainment from the northern and southern gyres. In the South Atlantic Bight, the transport of the Gulf Stream is 30 Sv at 28°N and 28 Sv at 27°N; observational results for the Gulf Stream transport are 31.7 ± 3.0 Sv at 27°N (Leaman *et al.*, 1987) and 29.5 Sv at 25.7°N (Niiler and Richardson, 1973).

Figure 8 shows the crossing of the DWBC under the Gulf Stream near Cape Hatteras. The DWBC is the deep northern branch of the NCG. Part of the DWBC turns cyclonically at 68°W; however the remainder continues southward along the slope. It is generally accepted that an interaction occurs between the Gulf Stream and the DWBC (Hogg, 1986; Pickart and Smethie, 1993; Pickart, 1994). As shown by Hogg and Stommel (1985), using
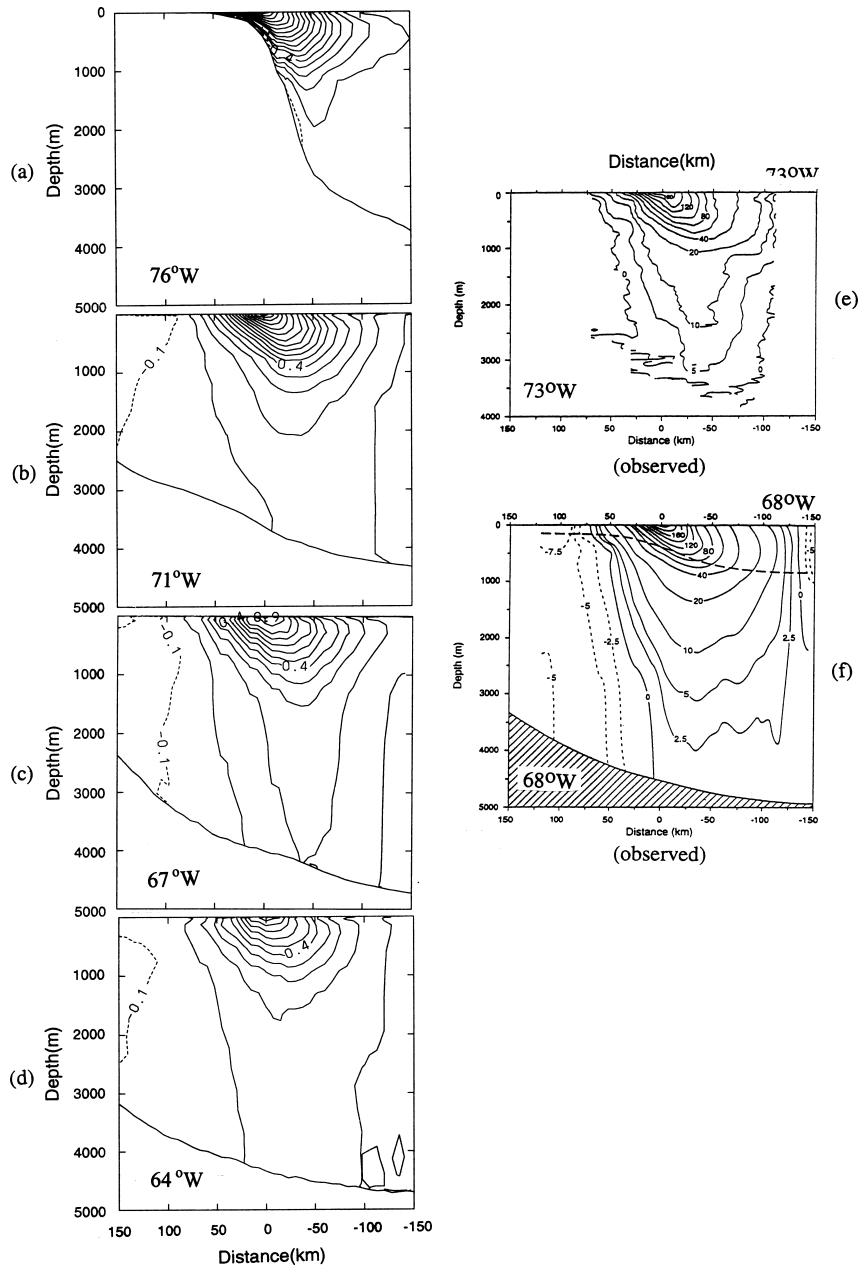
Fig. 9. Ensemble averaged downstream velocity distribution for two years (year 5 and 6) along stream coordinates sampled on the last day of 24 months at (a) 74°W, (b) 72°W, (c) 67°W, (d) 61°W, the longitude corresponding to the surface maximum velocity and observed results at (e) 73°W (from Halkin and Rossby, 1985), at (f) 68°W (from Johns *et al.*, 1995). Contour interval (C.I.) for (a) to (d) is 0.1 m s⁻¹, and for (e) and (f) is variable from 2.5 cm s⁻¹ to 20 cm s⁻¹. Dotted line represents negative values.

the potential vorticity conservation constraint, the DWBC moves downslope at its intersection with the Gulf Stream, a feature which is reproduced by the model as seen in the lower layer circulation; the crossing of the DWBC under the Gulf Stream occurs at 75°W. At the intersection, the DWBC which has flowed along the slope turns, crosses isobaths and moves to a deeper region.

The transport of the DWBC east of the Bahama Islands is approximately 20 Sv and feeds a deep cyclonic recirculation; this is in agreement with the observations of Lee *et al.* (1996). They carried out direct current observations for nearly six years in the eastern slope of the Bahamas and showed that the mean transport of the DWBC was 40 Sv east of the Bahamas together with a 27

Table 1. Volume transports of the Gulf Stream following the down stream coordinates, based on two year (year 5 and 6) ensemble averaged velocity fields of the model results. We adapt the definition of the transport according to Hogg (1992); the barotropic component is the integrated velocity below 1000 m plus the velocity at 1000 m times 1000 m. The baroclinic component is just the difference between the total transport and the barotropic component.

	76°W	73°W	71°W	67°W	64°W	62°W
Total (Sv)	49.9	65.8	78.6	101.5	64.0	48.4
Baroclinic (Sv)	38.7	31.3	32.7	28.3	24.4	17.3
Barotropic (Sv)	11.2	34.5	45.9	73.2	39.6	31.1
Barotropic/Total (%)	22.4	52.4	58.4	72.1	61.9	64.3

Sv deep recirculation. Thus, the DWBC transport of the model is less than the observed transport, but nonetheless reproduces the recirculation pattern east of the Bahamas and suggests that the path of the deep recirculation follows the 5000 m isobath (Fig. 2(b)).

3.4 Vertical structure

It is known from observation that the transport of the Gulf Stream increases rapidly downstream of Cape Hatteras (Knauss, 1969; Worthington, 1976; Halkin and Rossby, 1985; Hogg, 1992), but the profiles of the Gulf Stream in the upper layer (less than 1000 m depth) do not greatly change along the stream (Halkin and Rossby, 1985; Johns et al., 1995). Figure 9 shows a comparison of ensemble averaged model results for two years (year 5 and 6) with observations in vertical sections of the Gulf Stream along stream coordinates (Halkin and Rossby, 1985; Johns et al., 1995) wherein the origin is coincident with the maximum surface velocity axis. Model results (Figs. 9(a), (b), (c) and (d)) show that the jet structure of the Gulf Stream is maintained downstream of Cape Hatteras along the stream axis. Strong vertical shear appears at the cyclonic side of the Gulf Stream axis. The locus of maximum velocity shifts to the anticyclonic side with depth. These features are in good agreement with observations (Figs. 9(e) and (f)). However, the model surface maximum velocity is about 1.2 m s^{-1} and is less than that observed, about 1.8 m s^{-1}.

Downstream of Cape Hatteras, the model Gulf Stream maintains a baroclinic structure similar to the observations. The Gulf Stream has significant deep transport, and this barotropic component increases as far as 67°W. The downstream increase of the Gulf Stream transport is due to the barotropic components, the feature of which was shown from the observation results of Knauss (1969). As shown in Table 1, the total transport of the model Gulf Stream increases from 49.9 Sv at 76°W to 101.5 Sv at 67°W. This increase of the total transport is mainly due to the increase of the barotropic component (defined by the reference velocity of 1000 m depth, from Hogg (1992)) from 11.7 Sv to 73.2 Sv, even though the

baroclinic components actually decreases from 38.7 Sv to 28.3 Sv while the maximum core velocity decreases from 1.6 m s^{-1} at 76°W, 1.1 m s^{-1} at 67°W.

The average total transport of the model Gulf Stream is 101.5 Sv near 67°W, and this is between 113 Sv of Jones et al. (1995) at 68°W and 95.5 Sv of Hogg (1992) at 68°W, based on direct current moorings. The model transport near 73°W is 65.8 Sv and the transport increase between 73°W and 67°W is 5.5 Sv per 100 km which is larger than the observational estimation by Jones et al. (1995) of 4.2 Sv per 100 km.

According to the analysis of Hogg (1992), the total transport of the Gulf Stream is about 150 Sv near 65°W and this amount is maintained to 50°W. The model transport west of the New England seamounts decreases rapidly to 64.0 Sv at 64°W and 48.4 Sv at 62°W. This means that the NCG and the Worthington Gyre reproduced by the model is weaker than observations west of 65°W, probably due to the eastern boundary of the model along 55°W. The ratio of the barotropic components to the total transport increases monotonously to 72.1% near 67°W. West of 65°W the ratio is more than 60%, and this is consistent with the observational result of 67% at 61°W (Jones et al., 1995), even though the model transport decreases rapidly in this region.

Figures 9(a), (b) and (c) show the ensemble average velocity profiles for the two years (years 5 and 6) in stream coordinates at 73°W, 71°W and 67°W, the longitude corresponding to the maximum surface velocity. Velocity components are reckoned normal and parallel to a plane normal to the maximum velocity vector at the surface. Figure 10(d) shows observational average profiles from the Synoptic Ocean Prediction (SYNOP) central array; 67–70°W, 36.5–39°N (Johns et al., 1995). Near Cape Hatteras, the downstream maximum velocity of the model surface layer (50 m depth) is 1.6 m s^{-1} and the maximum velocity decreases with depth and shifts to the anticyclonic side of the Gulf Stream. The maximum velocity, 0.22 m s^{-1} at 1000 m depth, is on the anticyclonic side, 45 km from the axis. The width of the model Gulf Stream is about 200 km, independent of water depth. The maximum ve-
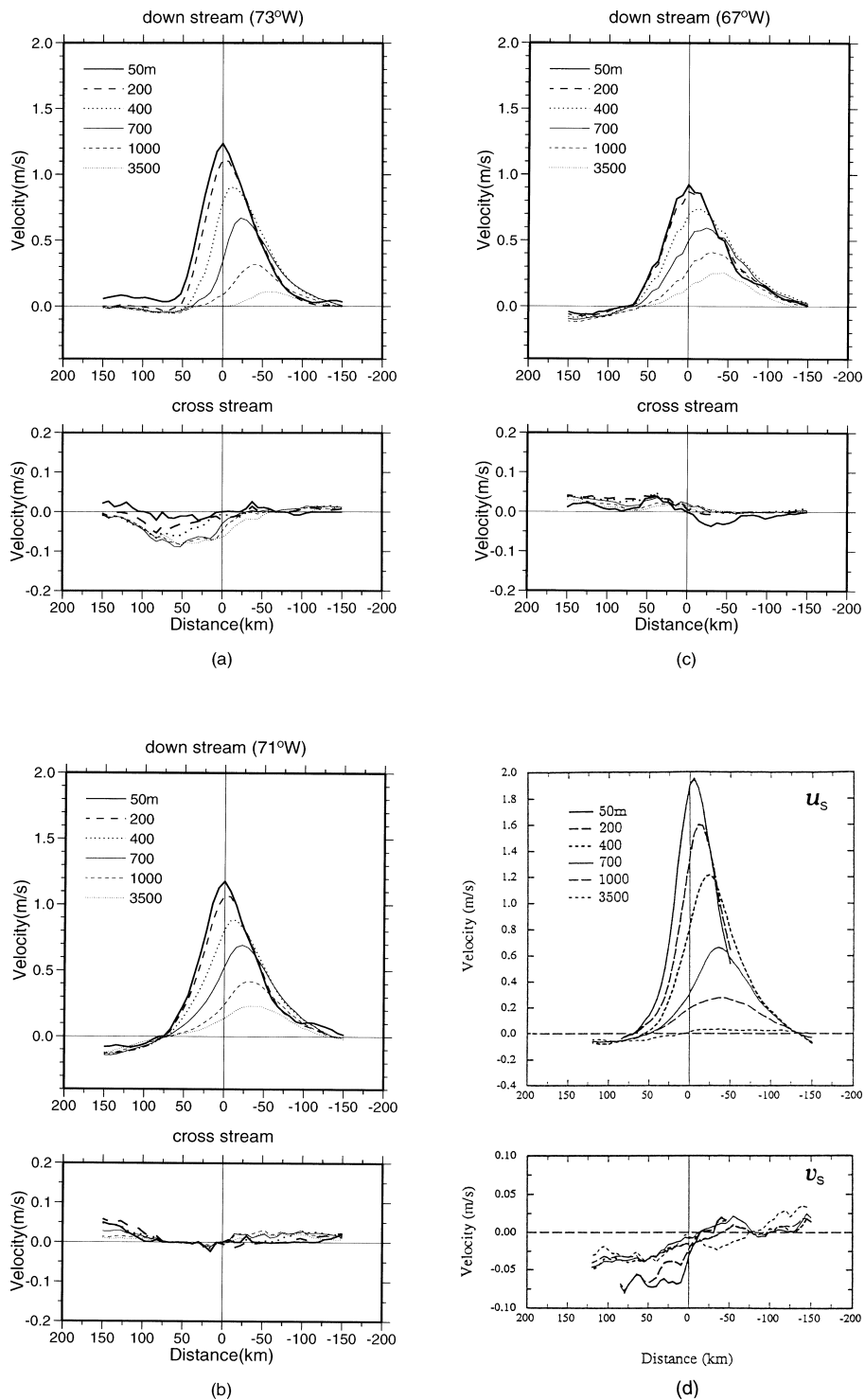
Fig. 10. Ensemble averaged down-stream (upper) and cross-stream (lower) velocity profile for two years (year 5 and 6) of the stream coordinate at (a) 73°W, (b) 71°W, and (c) 68°W, the longitude corresponding to the maximum surface velocity, and an observational average profiles (d) of the Synoptic Ocean Prediction (SYNOP) central array; 67–70°W, 36.5–39°N (Johns *et al.*, 1995).
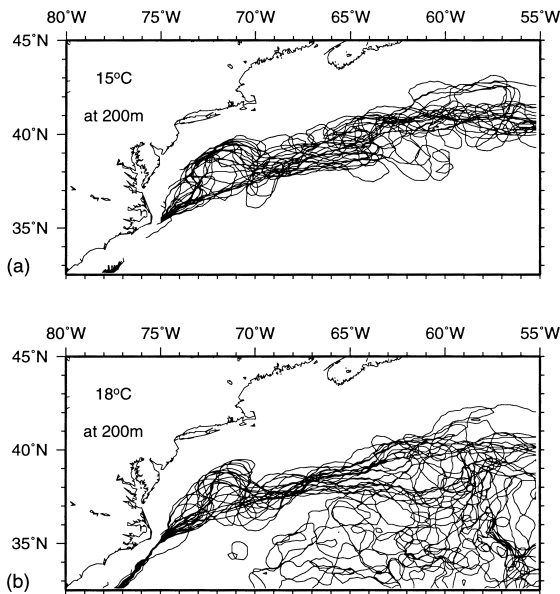
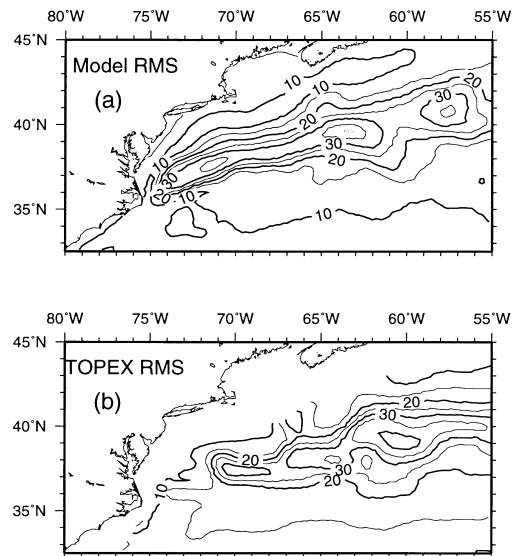Fig. 11. (a) 15°C isotherm and (b) 18°C isotherm at 200 m depth during the first four year simulation.

Fig. 12. (a) Distribution of RMS elevation anomaly of the model results and (b) RMS sea surface height anomaly of the TOPEX altimetry data from October 1992 to June 1996. C.I. is 5 cm.

locity at each water depth shifts to the anticyclonic side for the surface current core. The velocity at 3500 m depth is either negative or very low.

Cross stream velocity profiles (lower panel Fig. 10(a)) show that the convergence into the Gulf Stream, $\partial v_s/\partial y < 0$, occurs on the cyclonic side of the Gulf Stream. This means that the model transport increase of 5.5 Sv per 100 km is mainly due to the entrainment of the NCG through the barotropic component.

Near 71°W the convergence becomes weak and the entrainment occurs on the anticyclonic side, related to the Worthington Gyre. The observational results by Johns *et al.* (1995) (Fig. 9(d)) show that the entrainment is fed from the NCG and the Worthington Gyre. In the model result near 67°W (Fig. 9(c)), however, divergence occurs, which results in a decrease of the model transport west of the New England seamounts.

The streamwise velocity component of the three locations is quite self-similar except that the velocity scale decreases with downstream distance. The maximum speed of the upper layer Gulf Stream (shallower than 400 m depth) decreases eastward (Fig. 10(c)); however the structure of the Gulf Stream profile is maintained. The comparison with observations (Fig. 10(d)) show that the model results successfully reproduce the characteristic structure of the Gulf Stream profile, the asymmetry of velocity profiles, the shift of maximum velocity with depth, and the width of the Gulf Stream; however, as noted previously, the maximum speeds are less than those observed.

3.5 Space and time variabilities

Figure 11 shows the Gulf Stream path represented by the 15°C and 18°C isotherms at 200 m depth during the first four years of simulation with surface forcing. The "node" of the meandering between 68°W and 70°W is reproduced by the model, in agreement with observations (Kontoyiannis and Watts, 1994; Watts *et al.*, 1995). The variability of the path increases both west and east of the nodal region. Another region of large variability of the path occurs near 61°W (Fig. 11(b)), upstream of the New England Seamount Chain, which is consistent with the analysis of the satellite images of Cornillon (1986). In Fig. 7, the model results clearly show that many cold eddies originate along the seamounts and propagate to the southwest, which seem to be guided by topographic waves (Thompson, 1977; Hogg, 1981; Ezer, 1994).

The RMS elevation anomaly obtained from the 6-year model results and TOPEX altimetry data observed between October 1992 and June 1996 are shown in Figs. 12(a) and (b), respectively. The maximum value of model RMS anomalies in the Gulf Stream extension region (0.38 m) and its pattern is consistent with the TOPEX altimetry data (Fig. 12(b)), except for the northeastern region of the Cape Hatteras, where the model RMS is higher than 30 cm but the observational result is lower than 15 cm. This discrepancy seems to be caused by the overshooting fluctuation of the model Gulf Stream in that region (Fig. 11). Maxima of the TOPEX altimetry RMS occur near 65°W and 60°W, which is similar to Geosat altimetry re-
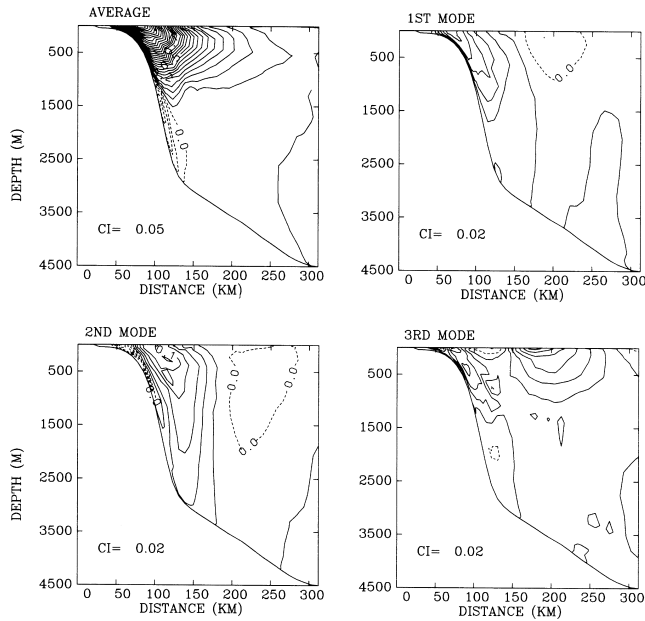
Fig. 13. Average fields and Empirical Orthogonal Functions (EOFs) for normal (alongshore) velocity through the section of 75°W. Proportion of the 1st mode EOF is 45.1%, the 2nd mode is 18.1% and the 3rd mode is 10.0%. Contour interval of the averaged velocity is 0.05 m s^{-1}. Dotted line represent negative values.
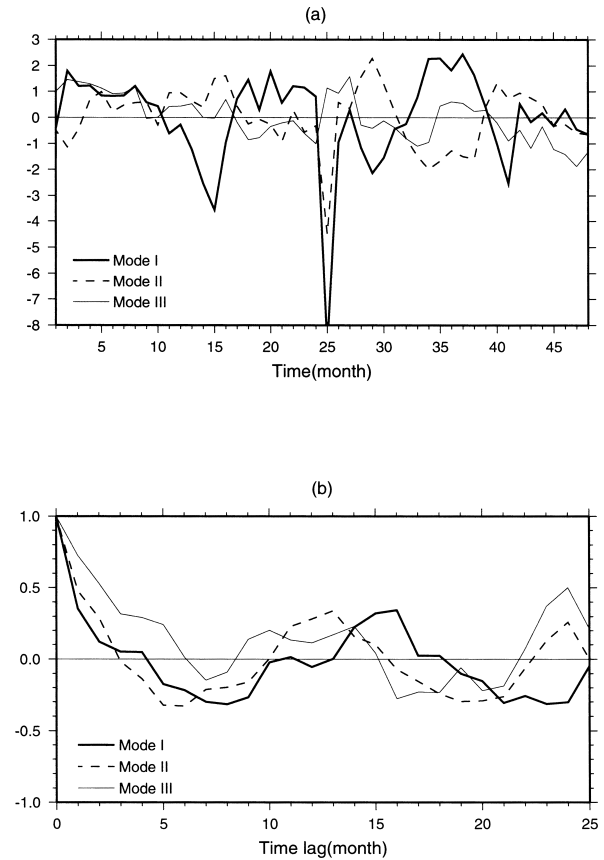

Fig. 14. (a) Time series of the first three EOF mode amplitudes for the normal velocity at the section of 75°W, and (b) the autocorrelation function of the EOF mode amplitudes.

sults (Ezer and Mellor, 1992). This distribution of RMS elevation anomaly is an improvement over previous numerical studies (Mellor and Ezer, 1991; Ezer and Mellor, 1992; Behringer, 1994). The maximum RMS anomaly from the model results (Fig. 12(a)) is near 63°W, and another peak of RMS anomaly occurs at 71°W. This result is quite similar to TOPEX and Geosat altimetry results.

Figure 13 shows the averaged normal velocity distribution and EOF patterns at 75°W near Cape Hatteras. The time series of EOF amplitude and the autocorrelation function of these time series are given in Fig. 14. The first EOF, which explains 45.1% of total variance, predominantly represents the offshore movement of the Gulf Stream. The second EOF mode shows a resemblance to the first EOF, except for the very narrow out-phase variability along the continental shelf break, which explains 18.1% of the total variance. The third EOF, which is 10.0% of total variance, has two peaks in the upper 1500 m layer; one is near shore and the other is offshore. This mode shows that the Gulf Stream and DWBC at Cape Hatteras are in-phase, in the sense that an increase (decrease) of the northward Gulf Stream velocity occurs with an increase (decrease) of the southward velocity of the DWBC. The time series of the first mode (Fig. 14) shows that a big negative peak occurs in month 25. This peak is due to the offshore movement of the Gulf Stream by the inter-

action of the warm eddy; in month 25 of the model simulation warm eddy intrudes between the Gulf Stream and the coast, and the Gulf Stream path is shifted off the coast by about 200 km. This peak is also shown in the second EOF. The autocorrelation functions (Fig. 14) indicate that the first three EOF modes have a near seasonal periodicity, which explain about 70% of total variance of the model Gulf Stream and the DWBC at Cape Hatteras.

Marchese (1999) showed a considerable seasonal variability of the Gulf Stream and its recirculation gyre by historical hydrographic data; the Gulf Stream position moves to the north in summer and to the south in winter. Tracey and Watts (1986) showed the evidence of the seasonal cycle of the Gulf Stream position and surface current speed near 73°W. The first three EOF modes of the model result suggest that there is a seasonal variability of the vertical velocity structure of the Gulf Streasm as well as its position near Cape Hatteras.

4. Discussion and Summary

Using the Princeton Ocean Model (Blumberg and Mellor, 1987; Mellor, 1998), a numerical simulation of
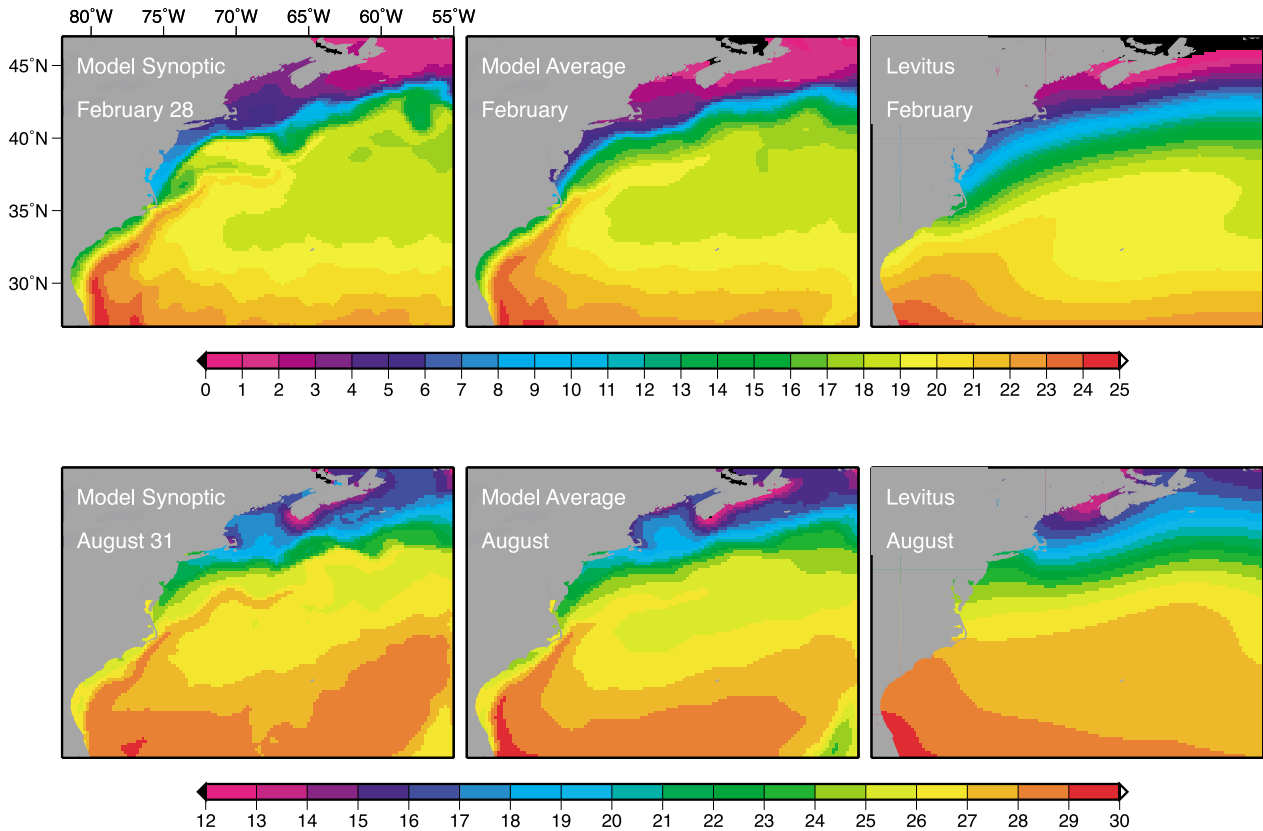
Fig. 15. Sea surface temperature (SST) distributions obtained from the synoptic model result of February 28 and August 31 of the sixth year (left), 6 year monthly averaged model result (middle) and the Levitus climatological data (right). Upper panels show the SST distributions in February and lower panels show the SST distributions in August. Unit of the color scale is °C.

the Gulf Stream system has been carried out; the model was forced with surface fluxes from the operational atmospheric Eta-29 km model. It has been shown that the surface fluxes of the model increase the northern cyclonic circulation, and play an important role in reproducing realistic Gulf Stream behavior.

The model, with surface fluxes, reproduces characteristic features of the Gulf Stream behavior with time. During the first year, disturbances of the Gulf Stream mainly occur east of 61°W, near the New England seamounts, and propagate to the west. A meander of the Gulf Stream then begins to appear at 72°W in the second year, and forms an overshooting of the Gulf Stream separation during the third year whereas, this overshooting is typical of Gulf Stream models and it can occur in nature. The simulation shows that the westward propagation of a cyclonic eddy plays a role in this transition of the Gulf Stream path. The observed Gulf Stream path is restored in the fifth and sixth years.

The travel time of the first mode Rossby wave from the eastern boundary to Cape Hatteras is about 2.5 years, which agrees with the time of the appearance of the over-

shooting pattern. One might speculate that the overshooting of the Gulf Stream path is related to the initial imposition of wind stress at the eastern boundary (Anderson and Gill, 1975) wherein the initial density field adjusts to the applied Eta wind fields when the signal from the eastern boundary arrives at the western boundary.

The crossing of the DWBC under the Gulf Stream is seen in the lower layer circulation (1000 m to bottom). The jet structure of the Gulf Stream is maintained downstream of Cape Hatteras along the stream axis. A strong vertical shear appears on the cyclonic side of the Gulf Stream, cross stream velocity profiles are barotropic and the convergence occurs mainly on the cyclonic side of the stream. The maximum speed of the Gulf Stream along the axis is less than the observed value. East of the Bahamas, the DWBC feeds the deep cyclonic recirculation, and suggests that this deep recirculation flows along the 5000 m isobath.

The RMS elevation anomaly of the model compares well with TOPEX altimetry data, and agrees with observations in terms of the distribution of the maximum RMS anomaly, implying that the meander and eddy activity of

the Gulf Stream is realistically reproduced by the model physics.

Thus far, we have not directly discussed the model's thermodynamic structure. Of course, since even the energetic Gulf Stream is nearly in geostrophic balance (Halkin and Rossby, 1985; Shay *et al.*, 1995; Watts *et al.*, 1995), the density structure is inferred from the velocity structure shown in this paper. However, we conclude the paper with Fig. 15, which shows the winter-summer seasonal variation produced by the model. Comparison of synoptic (left panels) and six year, monthly averaged model climatology (middle panels) illustrate the detail lost by averaging many synoptic realizations but where "data" is available at every grid point. The comparison of the model climatology and the Levitus climatology (right panels) illustrate the further loss of detail by the spatial averaging associated with the objective analysis scheme (Levitus, 1982) required by spatial scarcity of data. There is no Gulf Stream in the Levitus climatology, and other details in the South Atlantic bight are missing. (Note that there is now a 1/4° annual climatology (Levitus and Boyer, 1994) but seasonal variability is lacking.) None of these findings are surprising, but their quantification is instructive and may be a precursor to interactive observation-model analyses.

References

Aikman, F., III, G. L. Mellor, T. Ezer, D. Sheinin, P. Chen, L. Breaker, K. Bosley and D. B. Rao (1996): Towards an operational nowcast/forecast system for the U.S. East Coast. In *Modern Approaches to Data Assimilation in Ocean Modeling*, ed. by P. Malanotte-Rizzoli, Elservier Oceanogr. Series, **61**, 347–376.

Anderson, D. L. T. and A. E. Gill (1975): Spin-up of a stratified ocean, with applications to upwelling. *Deep-Sea Res.*, **22**, 583–596.

Beckmann, A., C. W. Böning, C. Köberle and J. Willebrand (1994): Effects of increased horizontal resolution in a simulation of the North Atlantic Ocean. *J. Phys. Oceanogr.*, **24**, 326–344.

Behringer, D. W. (1994): Sea surface height variations in the Atlantic Ocean: A comparison of TOPEX altimeter data with results from an ocean data assimilation system. *J. Geophys. Res.*, **99**, 24,685–24,690.

Blumberg, A. F. and G. L. Mellor (1987): A description of a three dimensional coastal ocean circulation model. p. 1–16. In *Three Dimensional Coastal Ocean Model, Coastal and Estuarine Sciences*, Vol. 4, ed. by N. S. Heaps, American Geophys. Union, Washington, D.C.

Cornillon, P. (1986): The effect of the New England Seamounts on the Gulf Stream meandering as observed from satellite IR imagery. *J. Phys. Oceanogr.*, **16**, 386–389.

Dengg, J., A. Beckmann and R. Gerdes (1996): The Gulf Stream separation problem. p. 254–290. In *The Warmwatersphere of the North Atlantic Ocean*, ed. by W. Krauss, Gebrüder Borntraeger, Berlin.

Ezer, T. (1994): On the interaction between the Gulf Stream and the New England Seamount Chain. *J. Phys. Oceanogr.*, **24**, 191–204.

Ezer, T. and G. L. Mellor (1992): A numerical study of the variability and the separation of the Gulf Stream, induced by surface atmospheric forcing and lateral boundary flows. *J. Phys. Oceanogr.*, **22**, 660–682.

Ezer, T. and G. L. Mellor (1994): Diagnostic and prognostic calculations of the North Atlantic circulation and sea level using a sigma coordinate ocean model. *J. Geophys. Res.*, **99**, 14159–14171.

Halkin, D. and T. Rossby (1985): The structure and transport of the Gulf Stream at 73°W. *J. Phys. Oceanogr.*, **15**, 1439–1452.

Hansen, D. V. (1970): Gulf Stream meanders between Cape Hatteras and the Grand Banks. *Deep-Sea Res.*, **17**, 495–511.

Hogg, N. G. (1981): Topographic waves along 70°W an the continental rise. *J. Mar. Res.*, **39**, 627–649.

Hogg, N. G. (1983): A note on the deep circulation of the western North Atlantic: its nature and causes. *Deep-Sea Res.*, **30**, 945–961.

Hogg, N. G. (1986): The northern recirculation gyre of the Gulf Stream. *Deep-Sea Res.*, **33**, 1139–1165.

Hogg, N. G. (1992): On the transport of the Gulf Stream between Cape Hatteras and the Grand Banks. *Deep-Sea Res.*, **39**, 1231–1246.

Hogg, N. G. and H. Stommel (1985): On the relation between the deep circulation and the Gulf Stream. *Deep-Sea Res.*, **32**, 1181–1193.

Johns, W. E., T. J. Shay, J. M. Bane and D. R. Watts (1995): Gulf Stream structure, transport, and recirculation near 68°W. *J. Geophys. Res.*, **100**, 817–838.

Knauss, J. A. (1969): A note on the transport of the Gulf Stream. *Deep-Sea Res.*, **16**, 117–123.

Kontoyiannis, H. and D. R. Watts (1994): Observations on the variability of the Gulf Stream path between 74°W and 70°W. *J. Phys. Oceanogr.*, **24**, 1999–2013.

Leaman, K. D., R. L. Molinari and P. S. Vertes (1987): Structure and variability of the Florida Current at 27°N: April 1982–July 1984. *J. Phys. Oceanogr.*, **17**, 565–583.

Lee, T. N., W. E. Johns, R. J. Zantopp and E. R. Fillebaum (1996): Moored Observations of Western Boundary Current variability and thermohaline circulation at 26.5°N in the subtropical north Atlantic. *J. Phys. Oceanogr.*, **26**, 962–983.

Levitus, S. (1982): Climatological atlas of the world ocean. *NOAA Prof. Pap.*, **13**, Natl. Oceanic and Atmos. Admin., Washington, D.C., 173 pp.

Levitus, S. and T. Boyer (1994): *World Ocean Atlas 1994 Volume 4: Temperature*. NOAA Atlas NESDIS 4, U.S. Department of Commerce, Washington, D.C.

Marchese, P. J. (1999): Variability in the Gulf Stream recirculation gyre. *J. Geophys. Res.*, **104**, 29549–29560.

Marshall, D. P. and C. E. Tansley (2001): On implicit formula for boundary current separation. *J. Phys. Oceanogr.*, **31**, 1633–1638.

Mellor, G. L. (1973): Analytic prediction of the properties of stratified planetary boundary layers. *J. Atmos. Sci.*, **30**, 1061–1069.

Mellor, G. L. (1996): *Introduction to Physical Oceanography*. AIP Press, Woodbury, New York, 260 pp.

Mellor, G. L. (1998): User's guide for a three-dimensional, primitive equation, numerical ocean model. *Prog. in Atmos. and Ocen. Sci.*, Princeton University, 41 pp.

Mellor, G. L. and T. Ezer (1991): A Gulf Stream model and an altimetry assimilation scheme. *J. Geophys. Res.*, **96**, 8779–8795.

Mellor, G. L. and T. Yamada (1982): Development of a turbulence closure model for geophysical fluid problem. *Rev. Geophys. Space Phys.*, **20**, 851–875.

Mellor, G. L., C. R. Mechoso and E. Keto (1982): A diagnostic circulation of the general circulation of the Atlantic Ocean. *Deep-Sea Res.*, **29**, 1171–1192.

Niiler, P. P. and W. S. Richardson (1973): Seasonal variability of the Florida Current. *J. Mar. Res.*, **31**, 144–167.

Pickart, R. S. (1994): Interaction of the Gulf Stream and deep western boundary current where they cross. *J. Geophys. Res.*, **99**, 25,155–25,164.

Pickart, R. S. and W. M. Smethie (1993): How does the deep western boundary current cross the Gulf Stream? *J. Phys. Oceanogr.*, **23**, 2602–2616.

Richardson, P. L. (1981): Gulf Stream trajectories measured with free-drifting buoys. *J. Phys. Oceanogr.*, **11**, 999–1010.

Richardson, P. L. (1985): Average velocity and transport of the Gulf Stream near 55°W. *J. Mar. Res.*, **43**, 83–111.

Shay, T. J., J. M. Bane, D. R. Watts and K. L. Tracey (1995): Gulf Stream flow field and events near 68°W. *J. Geophys. Res.*, **100**, 22565–22589.

Smagorinsky, J., S. Manabe and J. L. Holloway (1965): Numerical results from a nine-level general circulation model of the atmosphere. *Mon. Weather Rev.*, **93**, 727–768.

Spall, M. A. (1996a): Dynamics of the Gulf Stream/Deep Western Boundary Current crossover. Part I: Entrainment and recirculation. *J. Phys. Oceanogr.*, **26**, 2152–2168.

Spall, M. A. (1996b): Dynamics of the Gulf Stream/Deep Western Boundary Current crossover. Part II: Low-frequency internal oscillation. *J. Phys. Oceanogr.*, **26**, 2169–2182.

Teague, W. J., M. J. Carron and P. J. Horgan (1990): A comparison between the Generalized Digital Environmental Model and Levitus climatologies. *J. Geophys. Res.*, **95**, 7167–7183.

Thompson, J. D. and W. J. Schmitz (1989): A limited-area model of the Gulf Stream: design, initial experiments, and model-data intercomparison. *J. Phys. Oceanogr.*, **19**, 791–814.

Thompson, R. (1977): Observations of Rossby waves near site D. *Prog. Oceanogr.*, **7**, Pergamon, 1–28.

Tracey, K. L. and D. R. Watts (1986): On Gulf Stream meander characteristics near Cape Hatteras. *J. Geophys. Res.*, **91**, 7587–7602.

Watts, D. R., K. L. Tracey, J. M. Bane and T. J. Shay (1995): Gulf Stream path and thermocline structure near 74°W and 68°W. *J. Geophys. Res.*, **100**, 18291–18321.

Worthington, L. V. (1976): On the North Atlantic circulation. *Johns Hopkins Oceanographic Studies*, **6**, 110 pp.